

Material properties

Mechanical characterisation of Duraform® Flex for FEA hyperelastic material modelling

Shwe P. Soe^{a,*}

soes@cf.ac.uk

Nick Martindale^b

Chris Constantinou^b

Michael Robinson^a

^aCardiff School of Engineering, Queens Buildings, The Parade, Cardiff CF24 3AA, UK

^bBAE Systems, Advanced Technology Centre, Filton, Bristol BS34 7QW, UK

*Corresponding author. Tel.: +44 2920 874173.

Abstract

Laser Sintering (LS) is widely accepted as a leading additive manufacturing process with a proven capability for manufacturing complex lattice structures using a group of specially developed powder based materials. However, to date, very little research has been directed towards achieving greater knowledge of the properties of the elastomeric materials that can be used to produce energy absorbent items such as personalised sports helmets and running shoes via the LS technique. This paper will contribute to addressing this knowledge gap by examining the material properties and characteristics of Duraform® Flex, a commercially available elastomeric material used for such LS applications.

A 3D Systems HiQ machine fitted with a closed loop thermal control system was employed, together with a number of the advanced processing options available in the operating software. In order to measure the mechanical properties of this material, sets of ISO standard tensile test specimens were fabricated, employing a range of different manufacturing processing parameters. The result shows that varying key LS processing parameters such as powder bed temperature, laser power and the number of scanning exposures has a significant impact on the mechanical properties of the resulting part, including its ultimate strength and elongation at break. As LS is a layer manufacturing process, part properties are found to vary considerably between the horizontal (X-Y) and vertical (Z) build orientations.

The paper demonstrates how the measured tensile stress-strain curve can be transformed into appropriate hyperelastic material models **via employing** the data curve fitting process **employing in** PTC Creo 2.0 Simulate software, and how these material models can be used practically to match user requirements for the laser sintered parts, leading to design optimisation for both bulky solid and lightweight lattice components. The paper concludes with a discussion examining the potential future direction of the research.

Keywords: Additive manufacturing; Laser sintering; Duraform® Flex; Hyperelastic; Finite element analysis

1 Introduction

Over recent years, innovative examples have been documented in the literature about the translation of original design ideas, developed from either artistic imagination or functional expression, into physical parts via the LS process [1–5]. However, to date, the design and production of such parts has been primarily based on the use of nylon-12 powders, as a result of which a significant body of research focusing on developing an improved understanding of its material properties is available to support the design process [6–12]. Despite the ever increasing usage of the LS process, the range of materials available for this process is still very limited, especially when considering the vast array of materials available for injection moulding.

The most commonly used LS material is nylon-12, commercially offered by 3D Systems under the trade name of Duraform® PA [13], although similar nylon-12 based materials are also provided by other suppliers under different trade

names, including: EOS (PA2200), ALM (PA650) and EXCELTEC (Innov'PA 1550) [14–16]. Further variants, again based on nylon-12, utilise the addition of different types of fillers such as glass beads, or carbon-fibre to achieve stronger and stiffer materials [17–19].

In contrast, only three elastomeric materials are commercially available: Duraform® Flex from 3D Systems [20], TPE 210-S from Advanced Laser Materials (ALM) [21] and DESMOSINT™ X92A-1 from Lehman & Voss & Co [22]. Duraform® Flex is the main focus of this study and will be denoted simply as “Flex” hereafter. The material properties as listed on the respective material suppliers' datasheets are presented in Table 1.

Table 1 (Table 1 needs correction. Please see attached file for new Table options.) Material properties of LS elastomers.

Part orientation	Duraform® Flex	TPE 210-S	DESMOSINT™ X92A-1	
	Not specified	Not specified	X \rightarrow axis	Z \rightarrow axis
Tensile strength (MPa)	1.8	Not specified	27	22
Tensile modulus (MPa)	7.4	8	9	10
Elongation at break (%)	110	110	400	370
Shore A hardness	45–75	40	92	
Initial tear strength (N/m)	15–100	6000	Not specified	
Base material	Polyester	Nylon	Polyurethane	
Year of material released	2005	2005	2012	

According to the datasheets, Flex and TPE 210-S materials were released in 2005 whereas DESMOSINT™ X92A-1 was only recently introduced in 2012, all the materials aiming to meet a requirement for producing parts with rubber-like flexibility and durability. Typical applications of such parts include (1) prototyping and low volume manufacturing of athletic footwear, gaskets, hoses and seals, and (2) simulating thermoplastic elastomers, cast urethane, silicone and rubber parts and soft-touch over-moulded grips.

Additional information available on the datasheets of Flex and TPE 210-S suggests that a wide range of Shore A hardness can be achieved before and after infiltration but no details have been provided for corresponding LS processing parameters, nor for properties of infiltration materials and techniques employed. The datasheets of Flex and TPE 210-S do not specify in which orientation the specimens were fabricated but it is understood that the data reflects test pieces built along the primary scanning direction (X-axis) only.

The number of established thermoplastic elastomer (TPE) materials available for additive manufacturing (AM) by LS falls short of the six different ranges of thermoplastic elastomers developed for injection moulding [23]. Fig. 1 identifies these injection mouldable materials and demonstrates the range of hardness that can be accommodated by selection of the appropriate material. It is anticipated that development of further AM TPEs in the short to medium term will provide access to elastomeric materials with an increasingly wide range of properties.

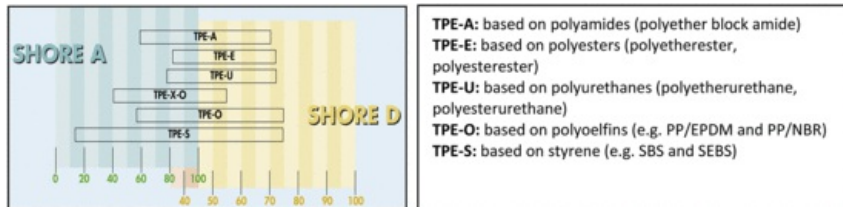


Fig. 1 Shore hardness of individual TPE group [23].

Selecting a material based on hardness data alone is, however, insufficient in practical terms for ensuring optimum design as hardness is generally only used for comparative study and quality control purposes. In most cases, additional rigorous testing needs to be conducted prior to subjecting the materials to the real life environment. To aid material selection, virtual prototyping is a step that can be taken to save time and cost before a commitment is made to full physical prototyping. Here, virtual prototyping implies the prediction of structural response through employing an appropriate finite element (FE) analysis tool.

This paper presents the range of stress and strain data achievable by employing different processing parameters, followed by the demonstration of a novel data curve fitting procedure used to derive material coefficients for

hyperelastic material modelling using PTC Creo 2.0 Simulate FE software.

2 Overview of LS machine and process capability for elastomeric powders

2.1 Equipment

The HiQ LS machine employed in the study is fitted with a 40 W CO₂ laser and has an X-Y build chamber size of 330 mm × 280 mm, and a maximum build height of 420 mm. When the machine was procured, the temperature control was configured as an open loop system. This system made it difficult to achieve a consistent powder bed temperature from build to build or along the Z height within a build. Such temperature variation was found to affect part quality producing either a soft part at one extreme, or a caked build (part cannot be cleaned due to very hard surrounding powder) at the other extreme. The machine was subsequently upgraded to enable closed looped temperature control, integrated with a black body infrared calibrator. Manufacturing runs have been successfully completed for both Flex and TPE210-S powders with this revised, closed loop machine configuration.

2.2 Temperature calibration techniques

Since different LS machines possess different thermal characteristics, it is common practice to calibrate the powder bed temperature for a specific machine. Experience suggests that a temperature variation of 4–5 °C can exist from one system to another for the same powder. The powder bed temperature can be calibrated in two ways. The technique offered by 3D Systems is to raise the temperature by 1–2 °C (starting from the recommended temperature) in every 3–4 layers until glazing of the powder bed is observed. A temperature 12–15 °C lower than the glazing temperature is then selected. Alternatively, the technique offered by an alternative machine manufacturer, EOS, involves placing an array of (50 mm × 50 mm) cross shaped parts across the powder bed and starting the build 2–3 °C lower than the recommended temperature. After a few layers of build, the crosses are found to curl up, especially at the corners. The temperature is then raised by another 2–3 °C depending on the severity of the curling and another layer of crosses built. The build temperature is selected 1–2 °C above the point where no signs of curling are observed.

The method offered by EOS is preferred and applied in this research because, firstly, it is easier to observe the part curling than to spot glazing on the powder bed and, secondly, the crosses can be placed at any height and anywhere in the build (even when the machine is running), allowing the machine operator to monitor the temperature stability. Thirdly, this method is suitable for any new powder under research, even when there is a lack of prior knowledge regarding a suitable temperature range. From experience, all LS powders are temperature sensitive and 1–2 °C can have a significant impact on overall part quality. From a research point of view, full confidence can only be achieved when test data is obtained from a machine with full thermal stability.

2.3 Operating parameters

The operating parameters for each material offered by 3D Systems are readily available in the machine operating software (version 3.45). The process parameters provided for Duraform® Flex are used as a starting point, shown as the default values in Table 2, along with the experimental parameters employed in this research. Here it should be noted that the machine used for this work had an advanced feature vital to carrying out this research, namely the ability to allow multiple scanning exposures (up to 10). Another important feature is the ability to scan the part in both the X and Y directions in alternate layers, thus equalising part properties in each of these directions and ensuring similar shrinkage in both.

Table 2 LS process parameters – Duraform® Flex.

Parameters	Default value	Experimental value used
Laser power (W)	9	12–18
Scanning speed (mm/s)	5080	5080
Scan spacing (mm)	0.15	0.15
Number of scan exposures	1	1–4
Layer thickness (mm)	0.1	0.1
Powder bed temperature (°C)	153	151–156
Powder feed temperature (°C)	90	90
Roller speed (mm/s)	305	177–305
Hatch style	X and Y	X and Y

3 Experimental procedure

3.1 Build preparation

Unlike other LS materials such as Duraform® PA or Castform™ PS powders [13], new supplies of Flex powder are observed to be lumpy and slightly sticky. Continued observation suggests that both new and recycled powders need fresh sieving before use, as the powder becomes lumpy again during storage. It is also notable that the maximum recommended roller speed was nearly twice that for the Duraform® PA material. Due to the effect of static charge a trail of soft powder lumps was created on the powder bed immediately after the roller passed, however this did not seem to have a negative effect on the sintering process, indeed, trials using a lower roller speed were observed to create more lumpy powder. Therefore, the maximum roller speed was maintained for all test builds.

3.2 Test specimen details

Detailed information regarding dimensions and testing specifications for the tensile testing of rubber and TPE materials can be found in BS ISO 37:2011 [24]. The dimensions of the specimens used in these trials are shown in Fig. 2 which corresponds to BS ISO 37:2011 Type 1.

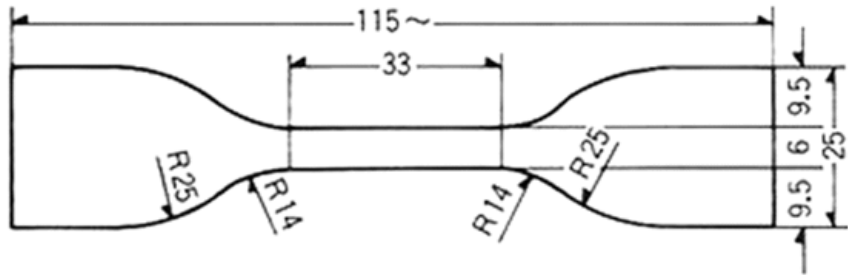


Fig. 2 (New Figure 2 is provided in attached file.) Detailed dimensions of the tensile specimen in mm (thickness, 2 mm).

3.3 Specimen fabrication

One of the objectives of this work is to evaluate the mechanical properties of parts using different build orientations. In this respect, the specimens are oriented in either the X-axis (horizontal) or Z-axis (vertical) of the build chamber, as shown in Fig. 3. Since an X and Y hatch scanning strategy has been applied, the part orientation along the Y-axis is equivalent to that of the X-axis, and is thus omitted in this study. To provide the data to support this project, more than 15 builds were carried out under a variety of conditions. As a starting point, the trial builds were based on the default processing parameters shown in Table 2. In later builds, several key parameters such as powder bed temperature, laser power and the number of scan exposures were varied depending on the test results observed from the prior builds. The laser power and number of scanning exposures are henceforth referred to as "LP" and "NSE" respectively. It was observed after each build that the remaining powder was slightly sticky, similar to the feel of a soft rubber part, and it was found to be easier to clean the parts as soon as the build was completed and remained hot, rather than allowed to cool to room temperature. An example of the fabricated tensile test specimens is shown in Fig. 4.

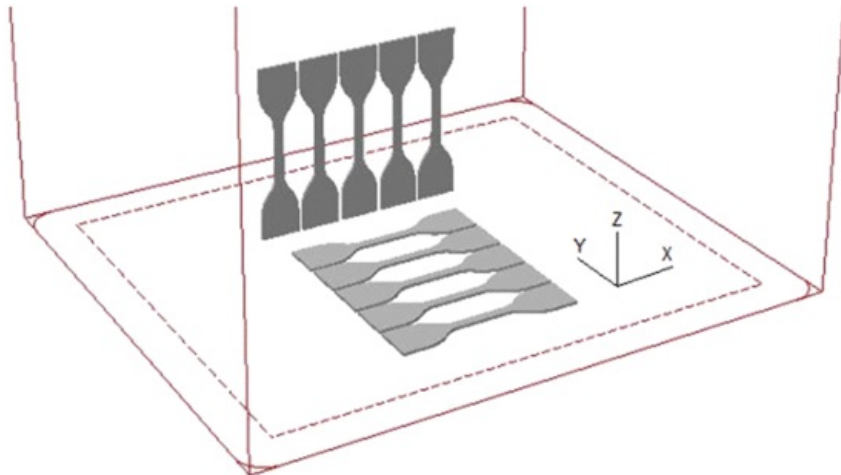


Fig. 3 Build layout of tensile specimens (X-axis and Z-axis).



Fig. 4 A fabricated tensile specimen.

3.4 Testing

Using a Shimadzu (AG-50kNG) mechanical testing machine, the fabricated tensile specimens (three for each process condition) were subjected to a quasi-static loading rate of 500 mm/min in accordance with the BS ISO 37:2011 recommendation [24]. Repeated loading cycles were also conducted so that the hysteresis effect and stress-softening behaviour for each cycle could be observed. During tensile testing, accurate strain data was recorded using digital image correlation.

4 Experimental results

Table 3 contains the process parameters and properties of tensile parts produced along the X and Z axes. Figs. 5–9 show the individual stress – strain graphs for samples processed under varying conditions, including different laser powers (i.e. 12 W, 15 W), the corresponding maximum number of scanning exposures (NSE 2 and NSE 4) and the orientation in which the parts were laid during the build (X and Z – axes). A range of repeated strain cycles from 10% to 600% are also shown, together with the results of a second, equivalent sample subjected to a single pull to failure.

Table 3 Process parameters and properties of parts produced in X-axis and Z-axis.

Laser power (W)	No of scanning exposures	Part orientation	Tensile strength at break (MPa)	Maximum elongation at break (%)
12	1	X	3.1	210
12	4	X	8.9	780
12	4	Z	5.7	200
15	1	X	4.2	270
15	2	X	7.8	660
15	4	X	12.5	780
15	1	Z	0.6	30
15	2	Z	4.1	100
18	1	X	5.5	380

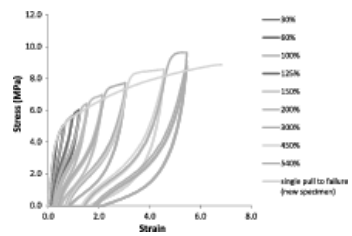


Fig. 5 Tensile stress-strain graph of two specimens showing repeated strain cycles and single pull to failure (LP 12 W, NSE 4, X axis).

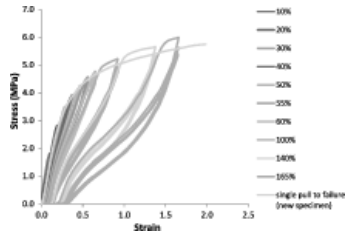


Fig. 6 Tensile stress-strain graph of two specimens showing repeated strain cycles and single pull to failure (LP 12 W, NSE 4, Z axis).

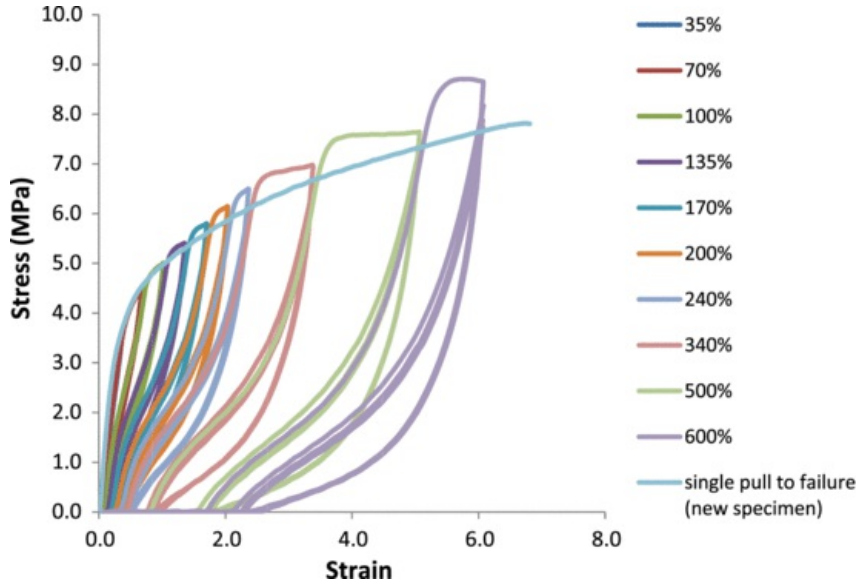


Fig. 7 Tensile stress-strain graph of two specimens showing repeated strain cycles and single pull to failure (LP 15 W, NSE 2, X axis).

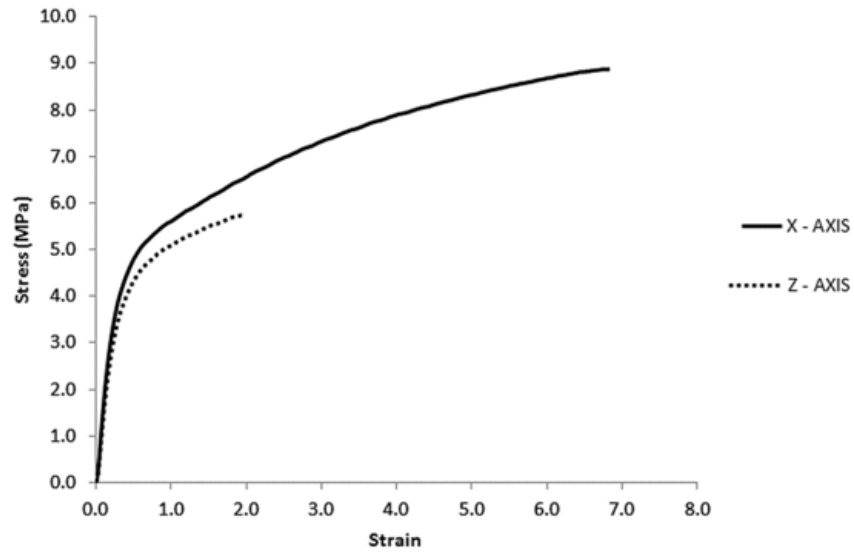


Fig. 8 Tensile stress-strain graph of two specimens (LP 12 W, NSE 4, X – axis and Z axis).

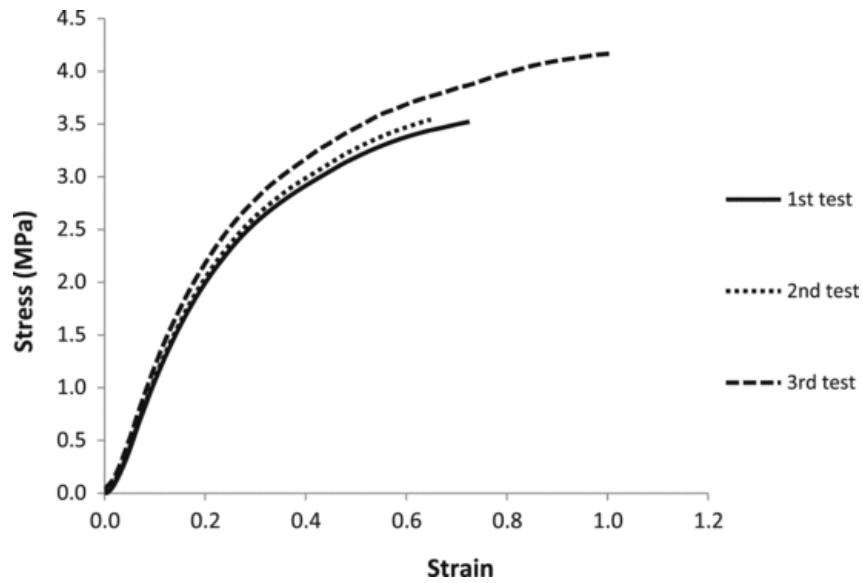


Fig. 9 Tensile stress-strain graph of three specimens showing the level of repeatability along Z axis (LP 15 W, NSE 2, Z axis).

5 Analysis of results

5.1 Effect of temperature


All the data shown in Table 3 and Figs. 5–9 were taken from test builds run with a fixed powder bed temperature of 155 °C. This temperature was chosen because earlier trials at lower temperatures, such as 153 °C, resulted in parts that were found to be very weak, especially in the Z-axis. In contrast, for higher temperature builds at 156 °C, difficulty was found in separating the parts from the hard surrounding powder. Since the aim of the study was to find the optimum processing parameters for building

lattice structure parts, a powder bed temperature of 155 °C was maintained as one of the optimum parameters and employed in all further experimental builds.


5.2 Effect of laser power and scanning exposure

Test parts were built to assess the effect of variation in the laser power and NSE. For all parts the powder bed temperature used was 155 °C. Three different laser powers; 12 W, 15 W and 18 W, were considered together with NSE up to 4.

In [Table 3](#), selected experimental results are shown in order to highlight the similarities and differences of the end properties achievable by varying the laser power and NSE. The values of tensile strength at break (TS_b) and elongation at break (E_b) with single exposures (NSE-1) shows that the parts produced at a laser power of 15 W have a higher TS_b and E_b than for 12 W. Similarly, those parts produced at a laser power of 18 W have higher TS_b and E_b than 15 W. However, under close inspection, the specimens fabricated with 18 W laser power were found to suffer from uneven thickness. In the case of the tensile bar specimens, the wider ends had an increased thickness compared to the narrower (middle) section. However, even the thickness increase in the middle section (compared to nominal 2 mm) was greater than the Z-offset compensation limit (0.25 mm) of the machine. On the basis of these observations, no further manufacture at 18 W was undertaken and evaluation of the effect of NSE, was based on 12 W and 15 W laser powers.

Study of the effect of the number of scanning exposures was limited to NSE  4. Although the machine software allows the use of an NSE up to 10, it was considered that:

- NSE up to 4 would be sufficient to show any trends
- We would intuitively expect any effect of increasing NSE to taper off at higher levels of NSE
- NSE has a direct impact on manufacturing time so there is a strong motivation to keep it as low as practicable.


It can be seen in [Table 3](#) that the TS_b and E_b increase dramatically as the NSE increases for all selected laser powers. Specifically at 12 W, both TS_b and E_b increased about 3 times when using an NSE of 4 compared to a single exposure (NSE  1). A similar trend can be seen for 15 W laser power, where the TS_b and E_b increase successively from a NSE of 1 to 2 and then to 4, although not in a linear fashion (the increases in structural properties diminishing with increasing NSE). It also shows that the use of increased NSE has a major impact on the properties of parts built in the Z-axis. Comparison of test results for parts manufactured with NSEs of 1 and 2 at a laser power of 15 W in the Z-axis, show the TS_b has increased seven times, where E_b has increased three times. The results indicate that there is a clear opportunity to customise the properties of the sintered material to meet specific requirements, based on careful selection of laser power and number of scan exposures.

The results suggest that the NSE value has a significant impact on the tensile strength and elongation at break, however there are also significant practical implications when considering the use of multiple scanning exposures. The first implication is that the time for sintering increases linearly with NSE, and this may limit the size and density of components that can be manufactured within realistic turnaround times. The second factor is that multiple scanning exposures can lead to part inaccuracy. This phenomenon can be related to the visual observation made during the sintering stage where, after the first laser exposure, the fluffy powder was seen to become level and dense. After the second exposure, the sintered area becomes darker and a shallow cavity is formed and found to get progressively deeper after each successive exposure, but at a reducing rate. The depth of cavity is also found to vary depending on the process parameters (NSE and LP) and the cross sectional area. As the powder is fluffy, the newly laid powder is unable to completely cover the deeper cavities and, as a result, the previously sintered layer is still transparent in some areas. In an attempt to remedy the problem, the powder feeding dosage and the roller speed were adjusted but no improvement was evident. As a result, the bottom of the part gets progressively thicker as NSE increases, which is a typical observation of those working with LS, who term this phenomenon “bonus-Z”, the severity of which is found to depend on the geometry of the part. Observation of fabricated parts suggests that a part with a large flat area can be covered with sticky caked powder at the bottom, whereas the round geometries (i.e. 3 mm diameter) which are built along the X-axis, can be seen to exhibit oval shapes. Although the Z-axis compensation limit of the machine may accommodate thickness changes of up to 0.25 mm, higher laser powers such as 15 W, in combination with the use of multiple scanning can increase such thickness variations up to 0.5 mm.

5.3 Effect of build orientation

[Fig. 3](#) depicts the orientation of parts manufactured in the X and Z-axis. The differences in the stress-strain characteristic between the two axes is significant, as shown in [Fig. 8](#), and this remains true for all combinations of processing parameters considered. This anisotropic characteristic should be taken into account in the design process. In addition, the use of increased NSE is a necessity to improve the overall performance of a part, particularly when the part is oriented along the Z-axis.

5.4 Build repeatability

[Fig. 9](#) shows the corresponding stress and strain curves of three parts, from the same build (LP – 15 W, NSE  2), aligned with the Z-axis. The curves demonstrate the variability of both TS_b and E_b between nominally identical parts, and highlight the level of repeatability in the part properties likely to be achieved. This variability is an inherent feature of the additive manufacturing process.

6 Relevance to design practice

6.1 LS design opportunities

Additive Manufacturing (AM) processes allow designers to express their design intent freely, not bounded by conventional manufacturing rules. The process has been supported by the development of specialist CAD software for building cellular lattice structures. These techniques enable the creation of biomedical scaffolds, surgical implants and strong, lightweight structures for applications in aerospace and motor racing [25–28].

The application of numerical optimisation techniques provides a means of developing efficient lattice designs. This process generally utilises FEA as a platform for the optimisation process and relies on the availability of accurate material data input. If the application involves the use of a hyperelastic material where large scale structural deformation is expected, then the decision as to which material model to use needs careful consideration. The following section explains how material test data is translated into a suitable hyperelastic material dataset using Creo Simulate software.

6.2 Hyperelastic material and FEA modelling

Hyperelastic material models are typically characterised by different forms of strain energy (density) functions [29]. These functions are expressed mathematically in terms of three stretched invariants or principle stretched ratios, derived from testing the material under different types of loading. In the Creo Simulate software six hyperelastic material models are supported which allow test data input of four different types of loading (uniaxial tension, equibiaxial tension, planar tension and volumetric compression, (i.e. hydrostatic pressure)) [30]. After entering the engineering stress and strain values, the software uses a Least Square Fitting Algorithm to calculate the material coefficients and provides an option to automatically choose the material model with the best fit based on the RMS error. If more than one test is entered, then the data from all of the tests are considered equally when determining the material coefficients. On completion of the analysis, the software reports true stress and true strain data [31].

6.3 Material model calibration

The calibration of models to represent the behaviour of hyperelastic materials is particularly challenging due to the effects of:

- Strain rate sensitivity
- Stress-softening
- Hysteresis

This is further complicated by material orthotropy introduced by virtue of the AM process.

The presence of these effects mean that a family of stress-strain curves would be required to fully characterise a material for a whole spectrum of loading scenarios.

In practice, limitations of the software, and availability of resource for testing, may restrict us to define the material behaviour with a single characteristic. Therefore, the approach adopted is to calibrate this model to the particular loading conditions likely to be encountered in the final application.

In the case of strain rate effects, this will mean undertaking material characterisation tests at a loading rate such that the strain rate seen in the specimen is in the same regime as that expected in the final application.

The stress-softening effect is illustrated in Figs. 5–7. These results are for a tensile specimen loaded quasi-statically to successively increasing strain levels, with no delay between load cycles, and for a second equivalent tensile specimen loaded to failure in a single pull. The figures show the material following a very different path on first loading (single pull to failure) compared to the re-loading cycles. In essence, the material exhibits different behaviour each time it exceeds the previously exercised strain range [29]. It is, therefore, important to base the calibration of the material model on test data corresponding to re-loading up to a particular peak strain level.

Apparent also in Figs. 5–7 is the material hysteresis, showing an increasing difference between loading and unloading curves as the strain level is increased. This provides a choice of which curve to calibrate against, loading, unloading or some combination of the two. In practice this choice will be dictated by the particular loading scenario of the final application.

The final consideration is how to account for the orthotropic nature of the material properties, those aligned with the build plane (X-Y axes) being significantly different to those aligned with the build height (Z-axis). The pragmatic approach is to adopt the properties corresponding to the principal loading direction in the final application. However it is recognised that this is rarely going to represent the true situation as most loading states will be fully 3D. Another alternative is to use a mean value, but clearly a better solution is to move up one level of modelling complexity and seek to adopt an orthotropic material model. This option is currently not available in the modelling software used in this study and is not considered further at this stage.

As an illustrative example, Fig. 10 depicts a particular loading cycle to 340% strain and shows the derivation of the equilibrium curve, based on the average of the loading and unloading curves and then offsetting this to pass through the origin. Similar equilibrium curves can be created for different strain cycles (Fig. 11), from which a suitable characteristic curve can be selected for the final application based on the level of strain envisaged.

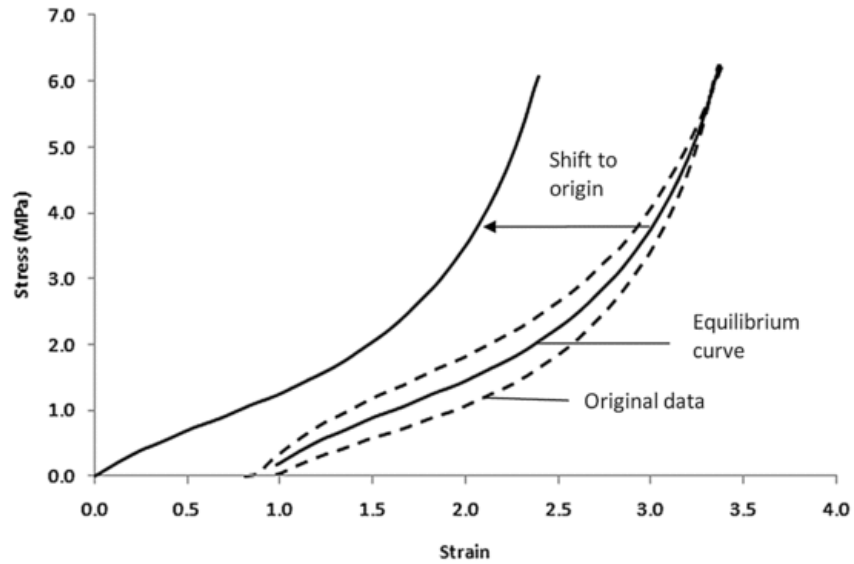


Fig. 10 Tensile stress-strain graph showing stabilised strain cycle of 340% strain (LP 15 W, NSE 2, X axis), its equilibrium curves (before and after move to origin).

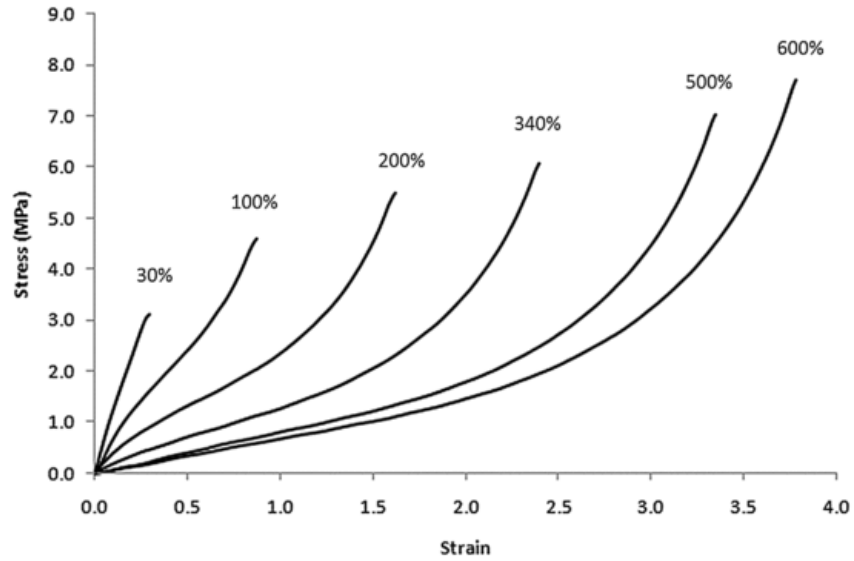


Fig. 11 Tensile stress-strain graph showing equilibrium curves (after shifting to origin) of selected strain cycles (LP 15 W, NSE 2, X axis).

In this study “Creo Simulate” FE software [30] has been used. This selects the most appropriate material model based on the stress-strain data entered, and calculates the material coefficients to achieve a best fit to the curve. In this case, the software automatically selects the “Yeoh” hyperelastic material model, as shown in Fig. 12, although alternative models could be selected by the user if required.

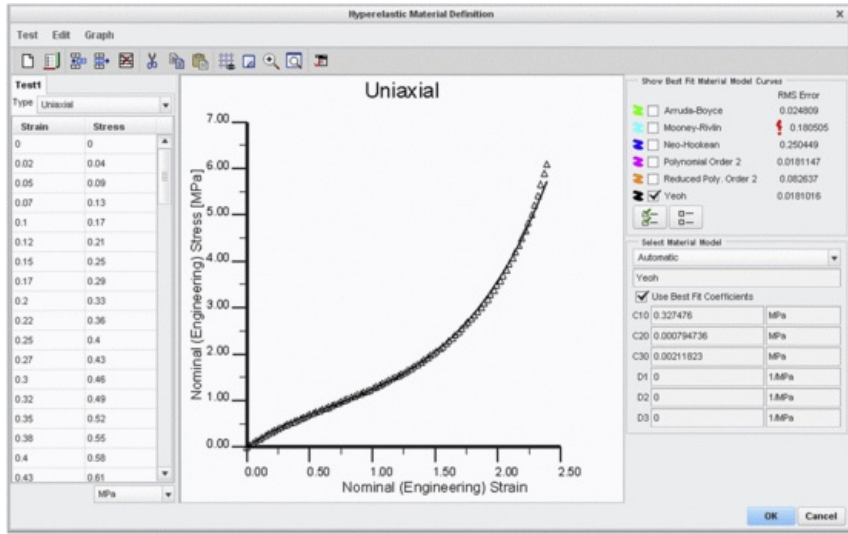


Fig. 12 Creo Simulate Hyperelastic Material curve fitting process window showing uniaxial stress and strain input (left), the fitted curve (middle), best fit material model and coefficients (right).

6.4 Model validation

In order to validate the material model, FEA was conducted to simulate the tensile test. The model was meshed with 3 mm shell elements throughout and constraints were applied to represent the clamping arrangements of the test machine. Loading was applied as a fixed velocity until a strain of 250% was achieved in the central gauge region of the specimen (Fig. 13). The FEA was run to capture the results for every 10% elongation.

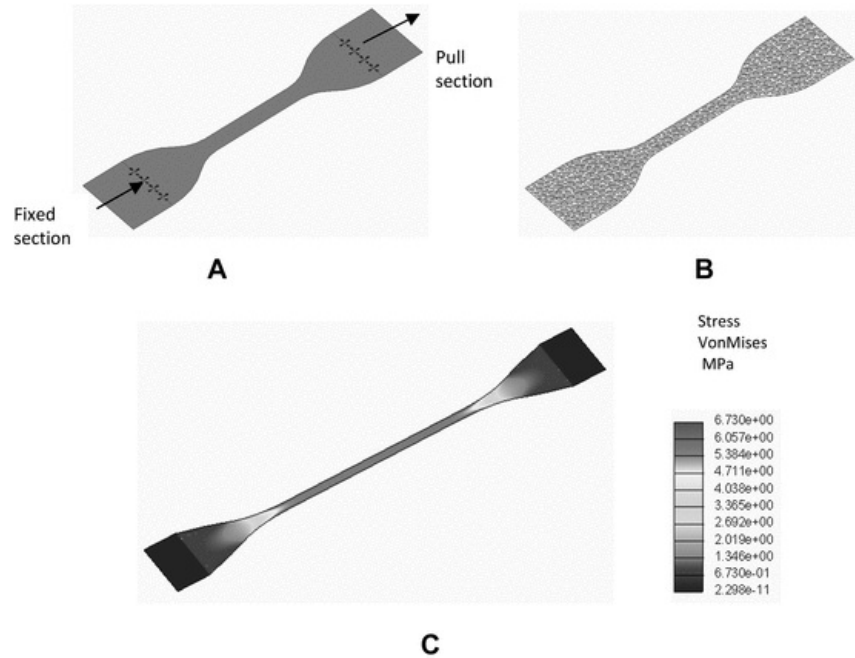


Fig. 13 (A) Model showing fixed end and pull end sections, (B) Fully meshed model (C) Deformed model showing VonMises (True) stress at 100% elongation.

Fig. 14 shows a comparison of the (engineering) stress-strain curve (converted from true stress-strain data) generated from FEA with the stress-strain curve from the experimental (engineering) stress-strain data. It shows that a high level of agreement has been achieved.

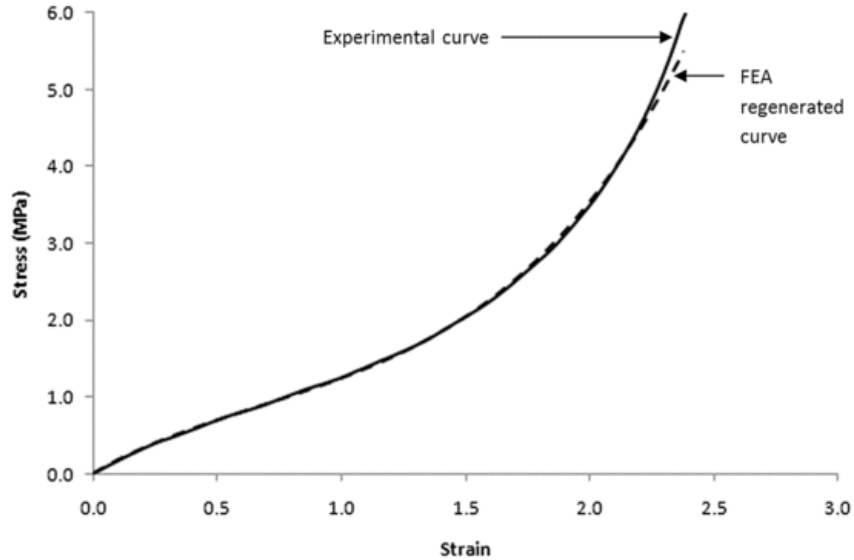


Fig. 14 A comparison of stress-strain (Experimental) curve vs. the FEA (Yeoh model) stress-strain curve.

7 Discussion and future research

In the previous section, it was shown that a material model can be derived which closely follows the experimental data, lending confidence that these material coefficients can be applied for the analysis of real designs to provide a means of assessing performance. Similarly, tensile curves for different load scenarios, materials or manufacturing conditions can be processed to provide corresponding material models and coefficients.

However, it is recognised that the current software limits applicability to loading scenarios that are predominantly uni-directional due to the assumption of isotropic properties, i.e. it will not account for the large difference between properties in the build plane direction compared to those along the build height. This large difference between the “in-plane” and “through-thickness” properties, combined with the modification to properties that can be achieved by alteration to the manufacturing process parameters provides huge scope for tailoring properties to meet specific stiffness and strength requirements. In addition, LS is a relatively flexible process since variable process parameters can be assigned on a part by part basis within a build, segment by segment basis within a part or on a layer by layer basis along the Z-height. This flexibility facilitates design optimisation in both solid and lattice components. Solid components can be divided into different volumes and different LS process parameters applied to each so as to achieve soft regions and hard regions wherever needed. The same approach may be applied to lattice components but, in addition, the element shapes, sizes, and densities of lattice structures can be altered to provide further opportunities to optimise structures.

In this study, the investigation of material properties has been limited to tensile data from both single pull and associated strain cycling tests. In future research, the authors intend to extend the range of tests to consider other types of loading such as biaxial, compression and planar.

A specific focus of future research will also be to extend these initial studies in order to develop an improved understanding on the life of the powder in relation to build time and build congestion, with the aim of better controlling part quality and maintaining build consistency.

8 Conclusions

The research identified that, while a range of TPE materials are available for use in the injection moulding process, the availability of TPE materials for LS remains comparatively limited. As a result, it is anticipated that as the range of TPE materials for LS increases in the short to medium term, so the range of available material properties will expand allowing a broader range of applications to be considered. In addition, the information available from the suppliers'

datasheets for the current materials was found to be insufficient for design purposes. This research was carried out to fill this knowledge gap by identifying and quantifying appropriate processing parameters following ISO standard procedures for rubber and TPE materials.

The HiQ machine integrated with a closed loop thermal management system was found to provide accurate temperature control. Using this system, a powder bed temperature of 155 °C was adopted as an optimum value. At this fixed temperature, the strength and elongation to break of the Flex material could be altered by modifying the number of scanning exposures and the laser power, either in combination or independently. However, it was found that there was an upper limit to the processing parameters above which part quality was sacrificed, typically a laser power >15 W combined with scanning exposures >2.

The Flex parts for all build orientations behave as typical elastomeric components in exhibiting stress-softening and hysteresis effects under repeated strain cycles. It has been demonstrated that, for a selected strain cycle, an equilibrium curve can be generated and FEA software used to obtain a suitable hyperelastic material model via the curve fitting procedure within the Creo Simulate software. A verification analysis showed that the FEA material model can closely replicate the experimental data.

This article aims to offer an interesting practical insight to both material suppliers and LS users into how a powder system with relatively unknown parameters can be systematically fine tuned to optimise its properties and parameters for processing, testing and verification. Likewise, it demonstrates novel ways for design engineers and FEA specialists to work collaboratively with material suppliers and LS practitioners in order to achieve improved outcomes from personalised manufacturing and high level rapid prototyping processes.

Acknowledgement

We would like to thank [BAE Systems, Advanced Technology Centre](#) for part funding the project upon which this article is based, for sharing their knowledge and in kindly giving us permission to present our experimental findings.

References

[1]

I. Gibson, D.W. Rosen and B. Stucker, *Additive Manufacturing Technologies: Rapid Prototyping to Direct Digital Manufacturing*, 2010, Springer.

[2]

C.K. Chua, G.K. Leong and C.S. Lim, *Rapid Prototyping: Principles and Applications*, 2010, World Scientific Publishing.

[3]

Materialise. MGX catalogue Available at: <http://www.mgxbymaterialise.com> (accessed 01.12.13).

[4]

3D Systems. Freedom of Creation Products Available at: <http://www.freedomofcreation.com> (accessed 01.12.13).

[5]

J.J. Crookston, A.C. Long, G.A. Bingham and R.J.M. Hague, Finite-element modelling of mechanical behaviour of rapid manufactured textiles, *Proceedings of the Institution of Mechanical Engineers, Part L: Journal of Materials Design and Applications* **222** (1), 2008, 29.

[6]

G.V. Salmoria, P. Klauss, R.A. Paggi, L.A. Kanis and A. Lago, Structure and mechanical properties of cellulose based scaffolds fabricated by selective laser sintering, *Polymer Testing* **28** (6), 2009, 648.

[7]

M. Vesenjāk, L. Krstulović-Opara, Z. Ren and Ž. Domazet, Cell shape effect evaluation of polyamide cellular structures, *Polymer Testing* **29** (8), 2010, 991.

[8]

H. Zarringhalam, N. Hopkinson, N.F. Kamperman and J.J.D. Vlieger, Effects of processing on microstructure and properties of SLS Nylon 12, *Material Science and Engineering: A* **435**, 2006, 172.

[9]

B.V. Hooreweder, F.D. Coninck, D. Moens, R. Boonen and P. Sas, Microstructural characterization of SLS-PA12 specimens under dynamic tension/compression excitation, *Polymer Testing* **29** (3), 2010, 319.

[10]

B.V. Hooreweder, D. Moens, R. Boonen, J.P. Kruth and P. Sas, On the difference in material structure and fatigue properties of nylon specimens produced by injection molding and selective laser sintering, *Polymer Testing* **32** (5), 2013, 972.

[11]

S. Dupin, O. Lamé, C. Barrès and J.Y. Charneau, Microstructural origin of physical and mechanical properties of polyamide 12 processed by laser sintering, *European Polymer Journal* **48** (9), 2012, 1611.

[12]

R.D. Goodridge, R.J.M. Hague and C.J. Tuck, Effect of long-term ageing on the tensile properties of a polyamide 12 laser sintering material, *Polymer Testing* **29** (4), 2010, 483.

[13]

3D Systems. Duraform® PA material datasheet. Available at: <http://www.3dsystems.com> (accessed 01.12.13).

[14]

EOS GmbH. PA2200 material datasheet. Available at: <http://www.eos.info> (accessed 01.12.13).

[15]

Advanced Laser Materials (ALM). PA650 material datasheet. Available at: <http://alm-llc.com/index.shtml> (accessed 01.12.13).

[16]

Exceltec. Innov'PA 1550 material datasheet. Available at: <http://www.exceltec.eu/product.html> (accessed 01.12.13).

[17]

R. Seltzer, F.M.D.I. Escalera and J. Segurado, Effect of water conditioning on the fracture behaviour of PA12 composites processed by selective laser sintering, *Materials Science and Engineering: A* **528** (22), 2011, 6927.

[18]

S. Kumar and J.P. Kruth, Composites by rapid prototyping technology, *Materials & Design* **31** (2), 2010, 850.

[19]

R.D. Goodridge, M.L. Shofner, R.J.M. Hague, M. McClelland, M.R. Schlea, R.B. Johnson and C.J. Tuck, Processing of a Polyamide-12/carbon nanofibre composite by laser sintering, *Polymer Testing* **30** (1), 2011, 94.

[20]

3D Systems. Duraform® Flex material datasheet. Available at: <http://production3dprinters.com/materials/duraform-flex-plastic> (accessed 01.12.13).

[21]

Advanced Laser Materials (ALM). TPE_210_S material datasheet. Available at: http://alm-llc.com/Tech_Data_Sheets/TPE_210_S.pdf (accessed 01.12.13).

[22]

Lehmann & Voss & Co. DESMOSINT™ X92A-1 material datasheet. Available at: <http://www.lehvoss.de/eng/1446.htm> (accessed 01.12.13).

[23]

Ticona. <http://tools.ticona.com/tools/documents/literature/2KENGLrev-101.pdf> (accessed 14.09.12).

[24]

BS ISO 37, Rubber, Vulcanized or Thermoplastic — Determination of Tensile Stress-Strain Properties, 2011.

[25]

J.Y. Tan, C.K. Chua and K.F. Leong, Fabrication of channelled scaffolds with ordered array of micro-pores through microsphere leaching and indirect Rapid Prototyping technique, *Biomedical Microdevices* **15** (1), 2013, 83.

[26]

Y. Jun and K. Choi, Design of patient-specific hip implants based on the 3D geometry of the human femur, *Advances in Engineering Software* **41** (4), 2010, 537.

[27]

Materialise. Magics 18 Software Available at: <http://software.materialise.com/magics-structures-module> (accessed 01.12.13).

[28]

Simpleware. +CAD Module Software Available at: <http://www.simpleware.com/software/cad-module.html> (accessed 01.12.13).

[29]

J.T. Bauman, Fatigue, Stress, and Strain of Rubber Components: A Guide for Design Engineers, 2008, Hanser Publishers.

[30]

PTC. PTC Creo Simulate 2.0 Software available at: <http://www.ptc.com/product/creo/simulate> (accessed 01.12.13).

[31]

R. Jakel, Analysis of Hyperelastic Materials with MECHANICA – Theory and Application Examples, 2010, PTC presentation for the 2nd SAXSIM at Technische Universität Chemnitz.

Queries and Answers

Query: The opening parenthesis does not have a corresponding closing parenthesis in the sentence “In the Creo Simulate software six...”. Please insert the parenthesis in the appropriate position.

Answer: a corresponding closing parenthesis is added.

Query: Please confirm that given names and surnames have been identified correctly.

Answer: All names and surnames are correct.